Applied Nanoscience (2023) 13:3289–3300
https://doi.org/10.1007/s13204-022-02745-7

ORIGINAL ARTICLE

Design of an innovative high-performance lead-free and eco-friendly perovskite solar cell

P. Arockia Michael Mercy[1] · K. S. Joseph Wilson[1]

Received: 30 July 2022 / Accepted: 9 December 2022 / Published online: 17 January 2023

Abstract

Perovskite solar cells (PSCs) with high efficiency and low cost are being actively developed. In recent years, the role of lead-based PSCs has become very important in the solar cell industry. But its toxicity and instability present a significant challenge to the development of commercially viable products. Under such circumstances, Ti-based all-inorganic (PSC) materials are of paramount importance in the development of high-performance PSCs. This work examines the theoretical feasibility of a lead-free, environmentally friendly, and reliable Cs_2TiBr_6-based PSC. The analysis of various hole transport layers (HTLs) and electron transport layers (ETLs) is performed in order to select materials that would result in stronger perovskite solar cells with higher stability. The goal of this paper is to design a lead-free PSC using Cs_2TiBr_6 as an absorber layer in the form of Au/$CuSbS_2$/ Cs_2TiBr_6/WO_3/FTO. Each composite layer is optimized and analyzed through simulations utilizing SCAPS-1D software to achieve elevated performance. A maximum power-conversion efficiency of 20.40% is achieved for the proposed solar cell through optimization of the ETL, HTL, metal contact materials, defect density of the absorber and the thickness of the absorber, HTL, and FTO. These results will pave the way for developing eco-friendly and highly efficient perovskite photovoltaic devices.

Keywords Lead-free perovskite solar cell · Numerical simulation · Cs_2TiBr_6 · $CuSbS_2$ · WO_3 · FTO

Introduction

Photovoltaic technology has been hailed as a promising technology for replacing depleted fossil fuels within the next few decades (Kabir et al. 2018). While solar cell technology has made tremendous advancements, the necessity for efficient, green, low-cost, and abundantly available materials remains a challenge (Jianbo Wang and Zhenming Xu 2017). Recent developments in materials which include their low cost, high stability, and simplicity of fabrication for new-generation solar cells have given rise to the most interesting topic (Mehrabian et al. 2021). The most widely available photovoltaic device is silicon solar cells, but their cost is high compared to conventional energy sources. It is obvious that cleanroom technology is required for Si to be used in photovoltaic applications, which greatly increases their inherent cost (Green 2009; Pizzini 2010). For solar cells, however, perovskite materials have shown high performance at very low costs, with their power-conversion efficiency (PCE) soaring from a few to more than 25% within a very short time frame, and they can be processed at room temperature (Kim and Kim 2021). Lead-based metal halide perovskites are attractive among these materials because of their high PCE. Halide perovskites (HPs) possess a triangular structure consisting of A, B, and X, where A represents a monovalent cation, B signifies a divalent metal cation, and X represents a halide anion (Md. Tohidul Islam et al. 2021). Essentially, these semiconductor materials display novel optoelectronic properties such as higher absorption coefficients, longer carrier diffusion distances, weakly bound exciton, and a wide bandgap tuning range (Alam and Ashraf 2020). Despite the improvement in PCE in PSCs, there remains a problem: the noxiousness of lead and the reality that the PSCs with the highest PCE consist of organic cations, like methylammonium and formamidinium ions (Alam et al. 2021). The ions in these materials are exceedingly volatile and hygroscopic, making the device heat and moisture intolerant. (Chen et al. 2018).The presence of lead in perovskites poses a threat to human health and the environment, which is a major concern

✉ P. Arockia Michael Mercy
arockiapackia@gmail.com

[1] PG and Research Department of Physics, Arul Anandar College, Karumathur, Madurai 625514, India

for their commercial applications (Babayigit et al. 2016). Scientists are, therefore, taking a great deal of interest in proposing and investigating lead-free perovskites for high-efficiency solar cells (Giustino and Snaith 2016).

Many of these materials exhibit promising photovoltaic responses. One of these is the cesium titanium (IV) bromide (Cs_2TiBr_6) compound (Chen et al. 2018). Recent research has identified Cs_2TiBr_6 as a promising compound in Pb-free perovskites. Also, photoluminescence suggests that the non-radiative recombination rate is low, and diffusion lengths above 100 nm have been observed. Thermal stress and exposure to light and humidity have also been reported to have a high level of stability. Cs_2TiBr_6 is a very excellent option for Pb-free perovskite solar cells due to its combination of numerous desirable features for solar energy applications (Wang et al. 2020). Lead-free and non-toxic Ti-based A_{2+1} Ti_{+4} X_{6-1} double perovskites have innovative optoelectronic applications (Slami et al. 2019). Cs_2TiBr_6, a direct-energy bandgap perovskite compound with excellent optical, electrical, and photovoltaic properties, has the potential to replace methylammonium lead halide perovskite in next-generation solar applications (Ju et al. 2018; Pecunia et al. 2020). Cs_2TiBr_6 is a tolerable and stable perovskite semiconductor because of its strong titanium (Ti) (Grandhi et al. 2021).

Design of novel perovskite solar cell

The structure of the multilayer Cs_2TiBr_6 solar cell employed in this investigation is shown in Fig. 1. The basic component of photovoltaic devices is an absorber layer, which captures photons and converts them into electron–hole pairs. The sandwich of two electrodes and an absorber layer may be sufficient for photovoltaic response,

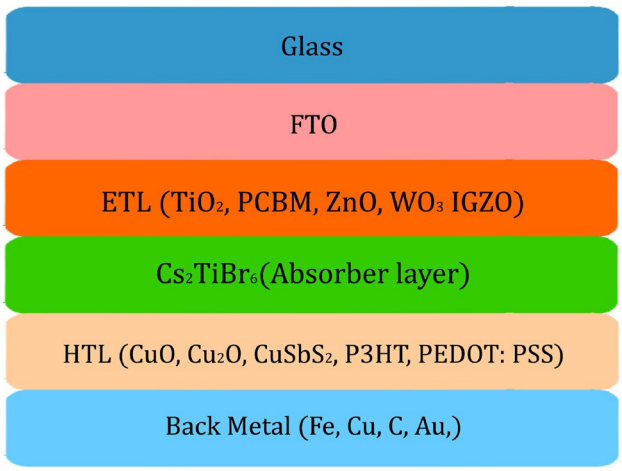

Fig. 1 Configuration of CS_2TiBr_6-based solar cell

but the best solar cell performance is achieved when electrons and holes are spread uniformly inside the photovoltaic system (Chen et al. 2016).

A PSC can be produced when the electron transport layer (ETL) and the hole transport layer (HTL) are sandwiched together for balanced charge distribution (Said et al. 2019). Cs_2TiBr_6 is chosen as an absorber layer. Both HTL and ETL must perform three well-defined tasks in terms of layer selection: (i) extract holes/electrons from the absorb layer, (ii) block opposite charges from entering the absorb layer to prevent recombination, and (iii) collect holes/electrons from the absorb layer and guide them to their appropriate electrodes (Pitchaiya et al. 2020; Gu et al. 2016).

It is well known that ETL and HTL materials are important in the extraction of electrons and holes from perovskite absorber layers. Some examples of such materials are CuO, $CuSbS_2$, Cu_2O, P_3HT, PEDOT: PSS. According to recent research, copper antimony sulphide ($CuSbS_2$) is a potentially earth-abundant photoelectric absorber and appropriate hole transport material for developing solar cells, because it promotes the absorption of solar radiation in cells, which in turn leads to energy production (Divya Sharma 2022; Atowar Rahman 2954; Shivesh et al. 2021; Yang et al. 2014). From the studies carried out here, $CuSbS_2$ has been identified as the most acceptable HTL among the other HTLs, for perovskite solar cells in terms of efficiency. Therefore, we opt $CuSbS_2$ as HTL for this study. In the literature, TiO_2 (Giordano et al. 2016), ZnO (Najafi et al. 2018), PCPM (Rai et al. 2020), WO_3 (Rai et al. 2020), IGZO (Mozhgan Kazemzadeh Otoufi 2020), are utilized as electron transport layer (ETM) in the photovoltaic cell. Because of its high efficiency compared to all other ETLs, WO_3 is regarded an ETL for perovskite performance. WO_3 offers several unique benefits of solution processing, outstanding electrical characteristics, and high mobility among these electron transport materials. The performance of perovskite is improved by employing WO_3 as an ETL (Rai et al. 2020). Here, WO_3 is made as an ETL in this study. The Au/$CuSbS_2$/ Cs_2TiBr_6/ WO_3/FTO perovskite solar cell is the optimum device.

Design and simulation

SCAPS software version 3.3.07, a one-dimensional (1-D) photovoltaic simulator created by ELIS, University of Gent, Belgium, was used in this investigation (Burgelman et al. 2000; Wang et al. 2020). To determine the density of electrons and holes individually, SCAPS 1D uses four different sets of equations (Verschraegen and Burgelman 2007). The following are the equations:

1. Differential form of the Poisson equation in terms of electrostatic potential is displayed below

$$\frac{d^2\phi(x)}{dx^2} = \frac{e}{\varepsilon_0\varepsilon_r}\left(p(x) - n(x) + N_D(x) - N_A + \rho_p - \rho_n\right),$$

where ϕ is the is the electrostatics potential, e is electronic charge, the permittivity of vacuum is ε_0, ε_r is relative permittivity, N_A stands for shallow acceptor impurity density while N_D stands for shallow donor impurity density. Similarly, ρ_p denotes hole density distribution and ρ_n denotes electron density distribution, with n (x) and p(x) denoting electron and hole density as a function of x.

2. The Continuity equation is given as follows

$$\frac{dJ_n}{dx} = G - R$$

$$\frac{dJ_p}{dx} = G - R,$$

where J_n and J_p represent the electron and hole current densities, G represents the generation rate, and R represents the recombination rate.

3. The electron and hole current densities are given by the Charge transport equation as follows

$$J_n = D_n\frac{dn}{dx} + \mu_n n\frac{d\phi}{dx}$$

$$J_p = D_p\frac{dp}{dx} + \mu_p p\frac{d\phi}{dx},$$

where μ_n is the electron mobility and μ_p is the hole mobility.

4. The absorption coefficient with respect to wavelength α (λ) can be calculated by the equation given below.

We use the following equation to get

$$\alpha(\lambda) = (A + \frac{B}{h\upsilon}\sqrt{h\upsilon - E_g},$$

where A, B are constant, h is plank constant, ν is frequency of photons and Eg is the band gap of the absorber layer. The band discontinuity between the interfaces of the different layers is small and therefore can be neglected for simplicity. The ambient temperature 300 K and the solar spectrum AM.1.5 (1000 W/m $^{2)}$ is used for this study. All of the physical and electrical parameters required by SCAPS 1D for each layer have been gathered from scientific literature and are listed in Tables 1 and 2 below.

Table 1 Photovoltaic device parameters used for these simulations are reported here, where doping concentration are just given for initial estimation which are optimized in later stages.

Results and discussion

This section includes an analysis of various HTLs and ETLs for an innovative device, as well as an optimizations of thickness of HTL, absorber, FTO and the optimization of absorber defect density for Cs_2TiBr_6 absorber.

ETL, HTL, Optimization for Cs_2TiBr_6 perovskite absorber

Figure 2 illustrates the performance of all device configurations with each HTL and ETL variation with standard thickness of 30 nm as given above in the literature (Tables 1 and 2), while keeping Au as back metal contact**.** The inorganic and organic materials such as CuO, $CuSbS_2$, Cu_2O, P_3HT,

Table 1 Input parameters of ETL

Parameter	FTO Saif (Ahmed et al. 2021)	ZnO (Huan et al. 2016)	WO3 (Mottakin et al. 2021)	PCBM (Lakhdar 2020)	TiO2 (Du et al. 2016)	IGZO (Lakhdar 2020)	$Cs2TiBr_6$ (Jani, et al. 2020)
Thickness(nm)	500	30	30	30	30	30	900
E_g(eV)	3.2	3.2	2.92	2	3.2	3.05	1.6
χ(Ev)	4.4	4.26	4.590	3.9	4.26	4.160	4.47
ε_r	9	9	5.76	4	10	10	10
NC(cm^{-3})	2.2×10^{18}	$2E^{18}$	$1.96E^{+19}$	$1E^{+21}$	$2E^{+18}$	$5E^{+18}$	$1E+^{19}$
NV(cm^{-3})	1.8×10^{19}	$1.8\ E^{19}$	$1.96E^{+19}$	$2E^{+20}$	$1.8E^{+19}$	$5E^{+18}$	$1E+^{19}$
μ_e(cm^2/V_S)	90	$2E+^{2}$	$1E^{+1}$	$1E^{-2}$	$2E^{+4}$	$1.5E^{+1}$	4.4E+0
μ_n(cm^2/V_S)	90	$5E^{+0}$	$1E^{+1}$	$1E^{-2}$	$1E^{+3}$	$2E^{-1}$	2.5E+0
Ve(cm/s)	1×10^{7}	1×10^{7}	1×10^{7}	1×10^{7}	1×10^{7}	1×10^{7}	1×10^{7}
Vh(cm/s)	1×10^{7}	1×10^{7}	1×10^{7}	1×10^{7}	1×10^{7}	1×10^{7}	1×10^{7}
ND(cm-3)	7×10^{20}	$1.5E^{+17}$	$3.68E^{+19}$	$1E^{+20}$	$6E^{+19}$	$1E^{+17}$	$1E^{+19}$
NA(cm-3)	0	0	0	0	0	0	$1E^{+19}$
N_t (1/cm^3)	1×10^{14}	1×10^{14}	1×10^{14}	1×10^{14}	1×10^{14}	1×10^{14}	1×10^{14}

Table 2 Input parameters of HTL

Parameter	CuO Zuo and Ding 2015)	$CuSbS_2$ Ameri et al. 2019)	Cu_2O Deepthi Jayan and Sebastian 2021)	P3HT Behrouznejad et al. 2016)	PEDOT:PSS Deepthi Jayan and Sebastian 2021)
Thickness (nm)	30	30	30	30	30
E_g(eV)	1.5	1.58	2.17	1.7	3.6
χ(Ev)	4.07	4.2	3.2	3.5	1.57
ε_r	18.1	14.6	7.1	3	3
NC(cm^{-3})	2.2×10^{19}	$2E^{18}$	$2.5E^{20}$	$2E^{+18}$	$2.2E+^{18}$
NV(cm^{-3})	5.5×10^{20}	$1\ E^{18}$	$2.5E^{20}$	$2E^{+19}$	$1.8E+^{19}$
μ_e(cm^2/V_S)	100	49	200	$1.8E^{-3}$	100
μ_n(cm^2/V_S)	0.1	49	8600	$1.8E^{-2}$	4
Ve(cm/s)	1×10^7	1×10^7	1×10^7	1×10^7	1×10^7
Vh(cm/s)	1×10^7	1×10^7	1×10^7	1×10^7	1×10^7
ND(cm-3)	0	0	0	0	0
NA(cm-3)	1×10^{15}	$1E^{+18}$	$1E^{+19}$	$1E^{+18}$	$2E^{+19}$
N_t ($1/cm^3$)	1×10^{14}	1×10^{14}	1×10^{14}	1×10^{14}	1×10^{14}

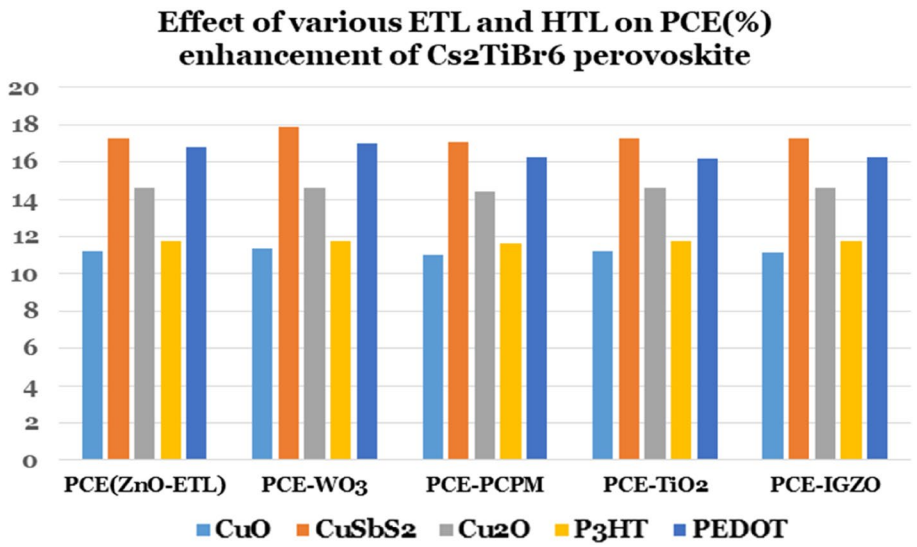

Fig. 2 Effect of various HTLs and ETLs on the variation of PCE for Cs_2TiBr_6

Table 3 Effect of ETL ZnO on J-V characteristics with various HTLs

HTLs on ZnO	V_{OC} (V)	J_{SC} (mA/cm^2)	FF (%)
CuO	0.653	24.3348	70.44
$CuSbS_2$	0.904	23.9519	79.85
Cu_2O	1.191	23.9306	51.25
P3HT	1.19	23.9554	41.31
PEDOT	0.820	23.9193	65.75

Table 4 Effect of ETL PCPM on J-V characteristics with various HTLs

HTLs on PCPM	V_{OC} (V)	J_{SC} (mA/cm^2)	FF (%)
CuO	0.653	24.1617	69.66
$CuSbS_2$	0.904	23.7817	79.2
Cu_2O	1.192	23.7599	50.84
P3HT	1.191	23.7687	41
PEDOT:PSS	0.804	23.6327	72.82

and PEDOT:PSS as Hole Transport Materials (HTMs) are analyzed on the design in the present work. The parameters associated with each HTMs are listed in Table 2. The J-V characteristics on various HTLs due to the effect of ZnO ETL are studied and given in Table.3. Similarly the effect of HTLs on various ETLs are also studied and are given in Tables 4, 5 and 6. From these analysis, it came to know that $CuSbS_2$ is a good HTL compared with other HTL

Table 5 Effect of ETL TiO2 on J-V characteristics with various HTLs

HTLs on TiO_2	V_{OC} (V)	J_{SC} (mA/cm^2)	FF (%)
CuO	0.653	24.33	70.49
$CuSbS_2$	0.904	23.9507	79.87
Cu_2O	1.192	23.9296	51.29
P3HT	1.191	23.94	41.36
PEDOT:PSS	0.884	23.9206	79.60

Table6 Effect of ETL IGZO on J-V characteristics with various HTLs

HTLs on IGZO	V_{OC} (V)	J_{SC} (mA/cm^2)	FF (%)
CuO	0.653	24.3315	70.38
$CuSbS_2$	0.904	23.9487	79.79
Cu_2O	1.191	23.9273	51.22
P3HT	1.19	23.9521	41.28
PEDOT:PSS	0.894	23.9387	78.69

Table 7 Effect of ETL WO3 on J-V characteristics with various HTLs

HTLs on WO3	V_{OC} (V)	J_{SC} (mA/cm^2	FF (%)
CuO	0.662	24.41	70.15
CuSbS2	0.905	23.95	82.57
Cu_2O	1.191	23.93	51.18
P3HT	1.19	23.96	41.21
PEDOT:PSS	0.864	23.91	79.8

combination on Cs_2TiBr_6 absorber PSC. Based on the J-V characteristics of the HTMs, which shows the Tables 3, 4, 5, 6 and 7, the product performance for each of the ETLs employed in the device. Performance is found to be very high for the configuration: Glass/FTO/WO_3/Cs_2TiBr_6/ $CuSbS_2$/ Au. The attained PCE is 20.90%, FF is 82.57%, J_{SC} is 24.9535 mA/cm^2, and V_{OC} is 0.9050 V.

The obtained results show that inorganic HTL improves the PCE of the device. Inorganic HTL has several advantages, including increased stability, excellent transparency, and band alignment. Multiple simulations were run to improve the ETL and HTL layers for PSC enhancement. The PCE variability of the Cs_2TiBr_6 PSCs using WO_3 as ETM and $CuSbS_2$ as HTM is found to be maximum.

Absorber layer thickness optimization

The thickness of the perovskite absorbing film plays a crucial role on the performance of solar cells. It has been discovered that if the film thickness is too thin, photons are poorly absorbed in the film, resulting in low PCE. If the film thickness is too thick, carriers recombine, resulting in reduced solar cell PCE. For the purpose of finding the optimal thickness of perovskite, multiple thicknesses of absorber have been simulated. Figure 3 depicts a graph of the PCE, and Voc, of PSCs, whereas Fig. 4 depicts a graph of the Jsc and FF properties of PSCs as a function of absorber thickness.

It is seen that all the solar cell output parameters improved greatly with the increase in absorber layer thickness. The

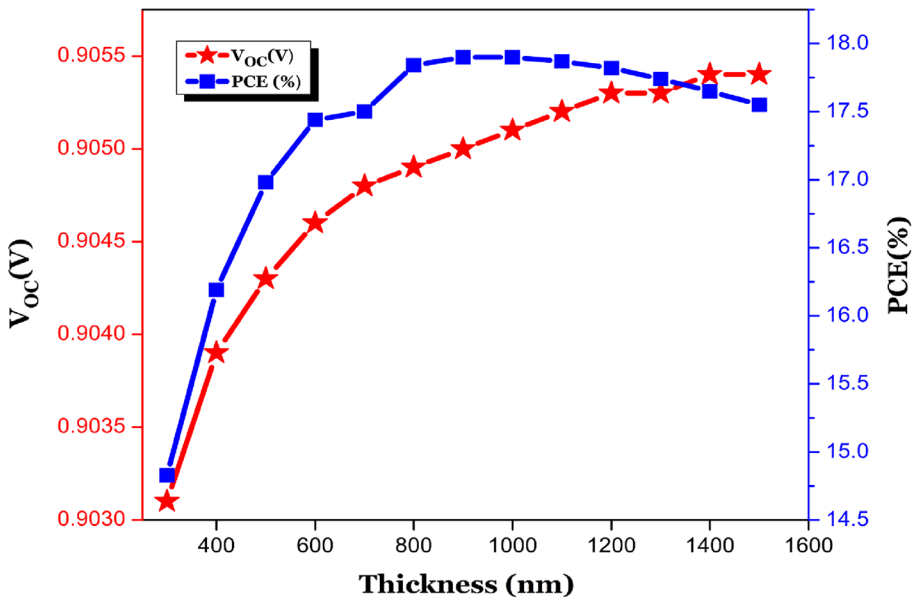

Fig. 3 Variation of V_{oc} and PCE with thickness of the absorber layer

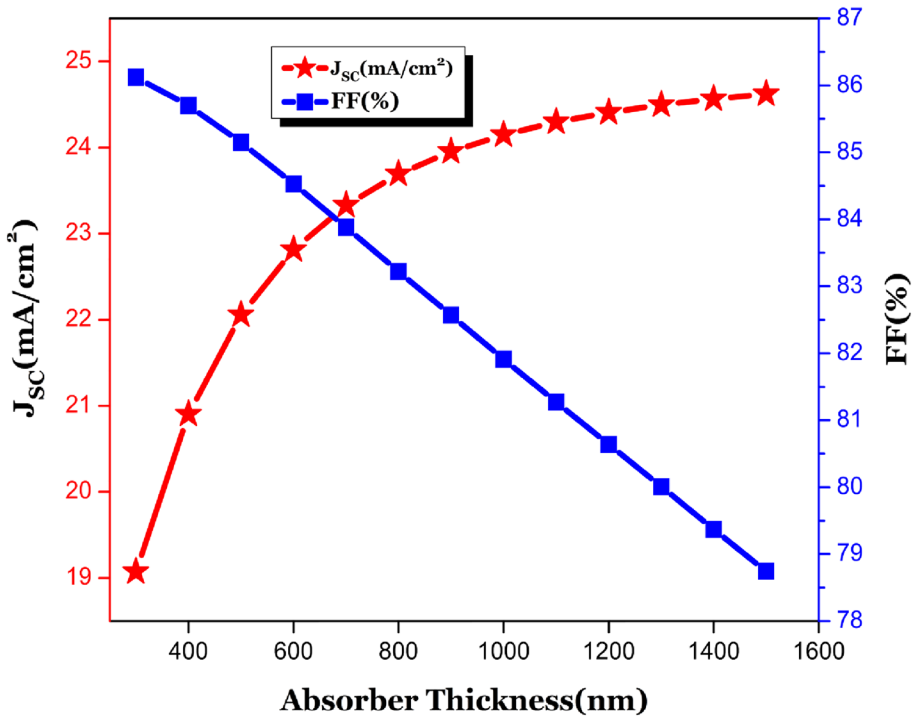

Fig. 4 Variation of J_{sc} and FF with thickness of the absorber layer

value of Voc is obtained to be 0.9030 V at 400 nm thickness and increases up to 0.905 V at 900 nm. It is also observed that Jsc increased linearly up to an absorber thickness of 900 nm and then almost saturated with increasing absorber thickness. Jsc of 23.9535 mA/cm^2 is estimated for a thickness of 900 nm. This is due to the increase in photon absorption with increasing thickness at a higher wavelength. Similarly, FF and PCE also increased with the increase in thickness. A FF of 82.57% is obtained at a thickness of 900 nm. The efficiency of the PSC is calculated 17.90% at a thickness of 900 nm. It can also be perceived from Figs. 3 and 4 that when the thickness exceeds 900 nm, all the photovoltaic parameters almost undergo saturation. This is due to the recombination of electrons and holes in the CS_2TiBr_6 layer before reaching the contacts. Thus, in the present work, the thickness of the absorber layer is optimized to be 900 nm, which is crucially important to reduce the charge recombination and hence improve the PV performance. At a perovskite optimized thickness of 900 nm, these graphs reveal a maximum PCE of 17.90%, Voc of 0.9050 V, Jsc of 23.9535 mA/cm^2, and FF of 82.57%.

HTL layer thickness optimization

Figure 5 displays the PSC performance analysis employing $CuSbS_2$ layer as an HTL that ranges from 30 to 90 nm in thickness. In the optimized thickness of 90 nm, PCE reached 18.38%. The V_{OC} and FF increase as the thickness increases, peaking of 0.9716 V and 78.67% at 90 nm, respectively, while the current density (Jsc) is 24.0448 mA/cm.^{2}

Effect of front electrode on PSCs performance

The performance parameters of PSCs parameters with ITO (Indium Tin Oxide) and FTO (Fluorine doped Tin Oxide) as the front transparent electrode are compared in J-V characteristics curves which are depicted in Fig. 6a, b. When the PCE is considered, it is visible that the FTO electrode is a better choice for this PSC to be a use to a solar cell than the ITO electrode.

Optimization of FTO layer thickness

The PSC performs much better when FTO is employed as the front electrode. Figure 7 exhibits PSC properties vs. FTO thickness within range of 50–550 nm. The FF, J_{sc}, V_{OC}, and PCE first increases rapidly with the FTO thickness. Therefore, the optimized FTO thickness is around 50 nm which gives V_{OC} of 1.02 V, J_{SC} of 20.13 mAcm-2, FF of 88.2% and PCE of 19.2%.

Optimization of absorber defect density

A key factor that has a substantial impact on device performance is the total defect density of the active layer. In addition to the increased recombination caused by the more defects in the absorber layer, the higher defect concentrations result in a faster rate of degradation of

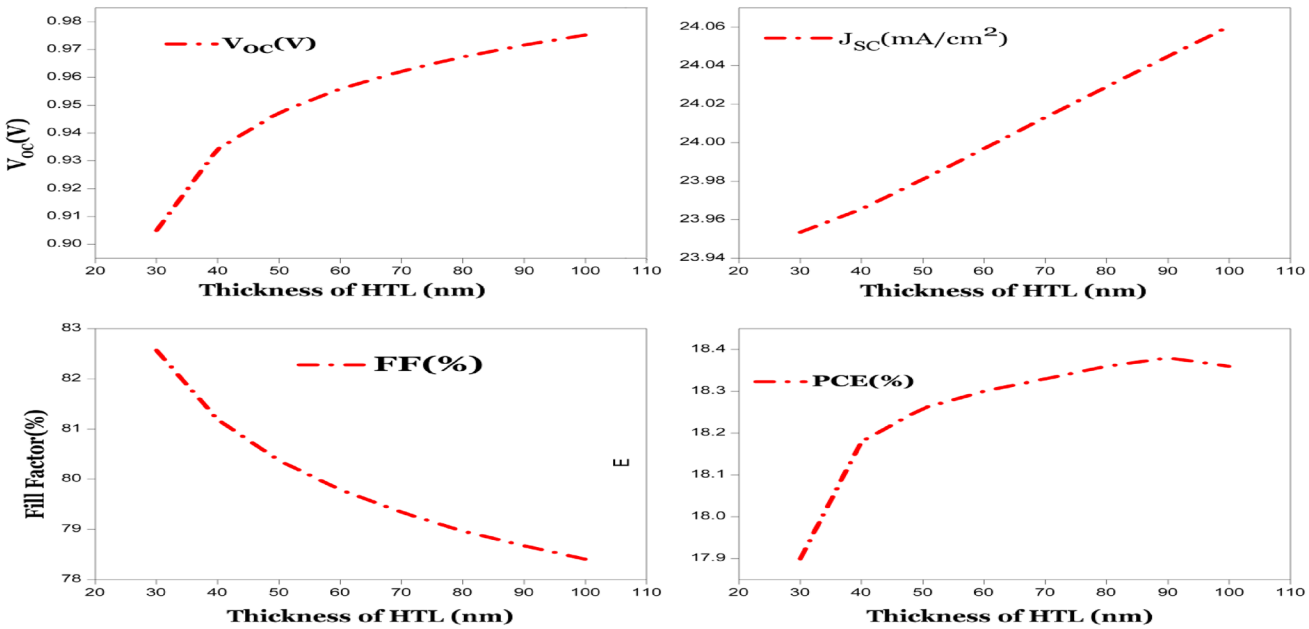

Fig. 5 Effect of HTL thickness on PSC performance characteristics

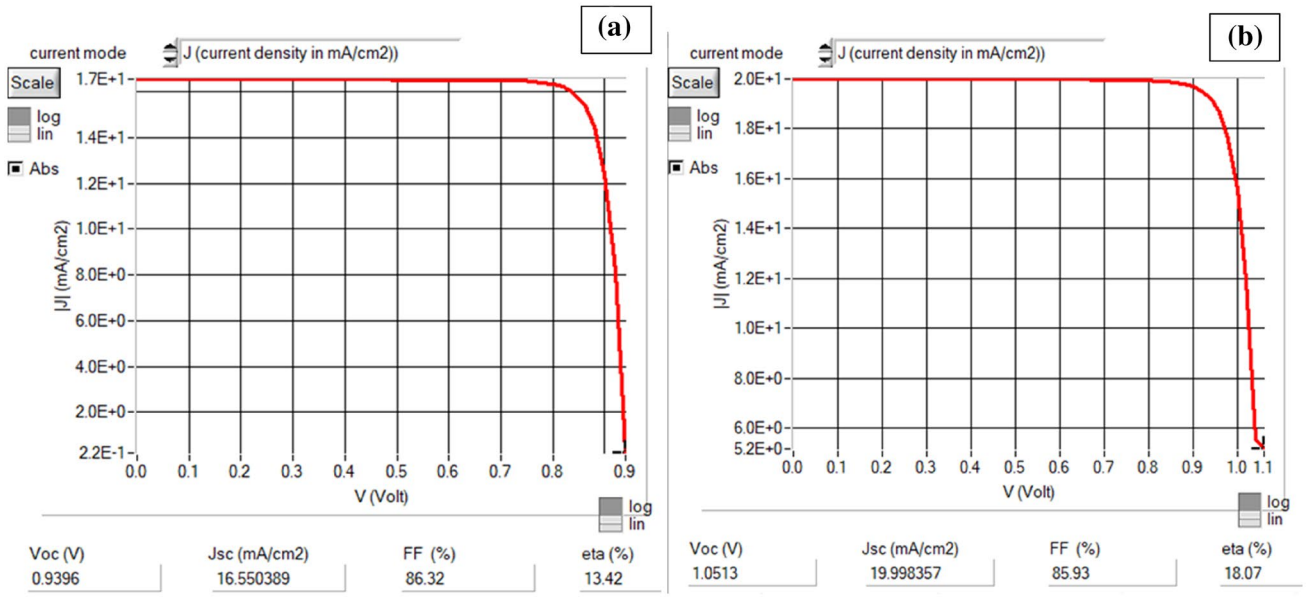

Fig. 6 Impact of (a) ITO and (b) FTO front electrode on PSCs performance

the film, reduced stability, and lower performance of the device (Ouslimane et al. 2021). Figure 8 shows the PCE, while Table 8 shows how the J-V characteristics of the design are affected by varying interface defect densities. The defect density of absorber interfaces is examined on a scale ranging from 10^{13} cm^{-3} to 10^{17} cm^{-3}. It is evident that all cell performances degrade as the number of defects increases in the absorber layer. There is a significant impact of defect density on FF and J_{SC}. A defect density of 10^{17} cm^{-3} results in a FF and J_{SC} as low as 28.44% and 15.0321 mA/cm^2 (Table 8). Additionally, as the defect density rises from 10^{13} cm^{-3} to 10^{17} cm^{-3}, the efficiency is drastically lowered from 20.4 to 3.06%. In terms of defect density, PSCs based on Cs_2TiBr_6 have the maximum PCE of 20.40% when compared to other defect densities as illustrated in Fig. 8. This table displays the outcomes of Voc, J_{SC}, and FF for various defect densities

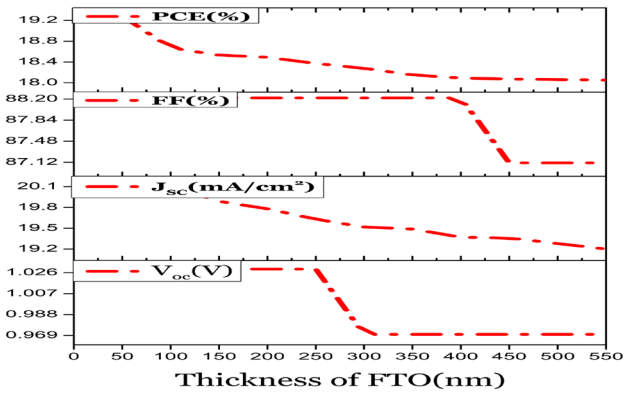

Fig. 7 Optimization of FTO thickness

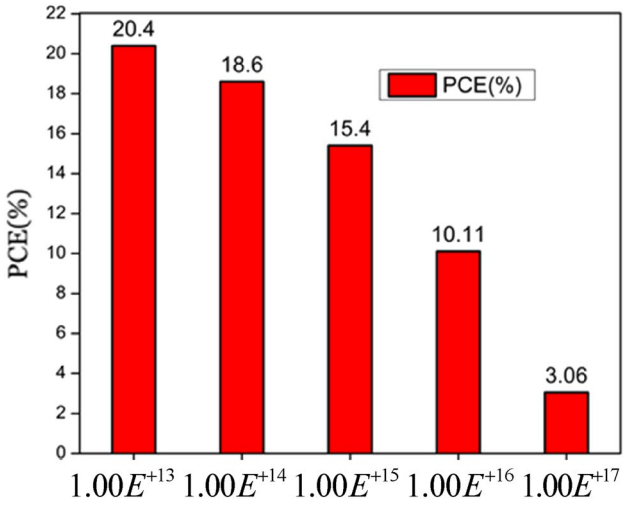

Fig. 8 Effect of absorber defect density on PCE

Table8 Effect of absorber defect density on J-V characteristics

defect density(cm^{-3})	V_{OC} (V)	J_{SC} (mA/cm^2)	FF (%)
$1.00E^{+13}$	0.9717	24.3404	86.24
$1.00E^{+14}$	0.9717	24.3201	78.68
$1.00E^{+15}$	0.9561	24.2022	66.53
$1.00E^{+16}$	0.86	23.1103	50.95
$1.00E^{+17}$	0.7165	15.0321	28.44

and it is found that the defect density corresponding to 10^{13} cm^{-3} has better solar cell parameters.

The impact of the rear metal work function on the PSC's execution

When the work function of a metal is larger, it can be represented as the amount of energy or photons efficient. Studies have found that solar cells become more efficient when their work functions are larger. When the work function value rises while the carrier's barrier height falls, the ohmic contact rises. PSCs have used a variety of metals as back contact electrodes, as shown in Table 9 with Fig. 9

Table 9 Different kinds of back metal contacts and its work

Back metal Zuo and Ding 2015)	Cu	C	Au	Fe
Work function (eV)	4.9	5	5.3	4.81

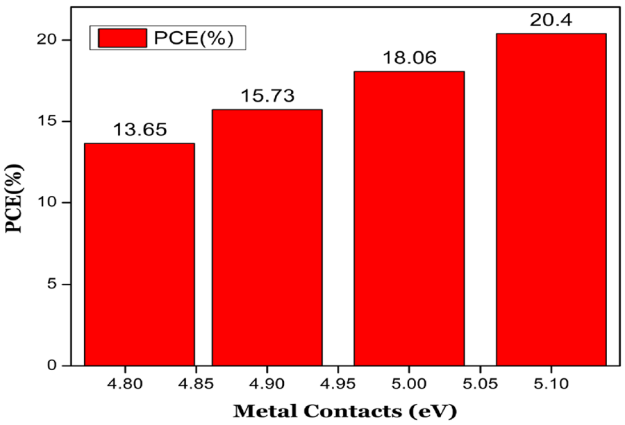

Fig. 9 Influence of various types of metal contacts on PSC's PCE

Simulations have been performed involving copper (Cu), iron (Fe), carbon (C), and gold (Au) as back contacts for PSCs. The ETL and electrode must be coupled in an Ohmic way for electrons to be collected to the load. It is appropriate for back contact materials to own a relatively high work function. In addition, as the work function of the back metal contact is reduced below 5.1 eV, the photovoltaic parameters gradually decline. Figure 9 shows that increasing the work function of the back contact materials improves the efficiency of PSCs. It reaches its maximum PCE of 20.4%, when its back contact is 5.1 eV. The best performing back electrode material is Au which proves the PCE curve of Fig. 9 that yields the V_{OC} of 1.5628 V, J_{SC} of 14.3404 mA/cm^2, and FF of 90.01%

The impact of temperature on PSC performance

Different geographical regions use solar cells at different occasion of the year with varying weather conditions and climates, which affect the operation temperature of the photovoltaics. Simulations were run at various operating temperatures to see how temperature affects PSC's execution. The effect of temperature change on the performance of

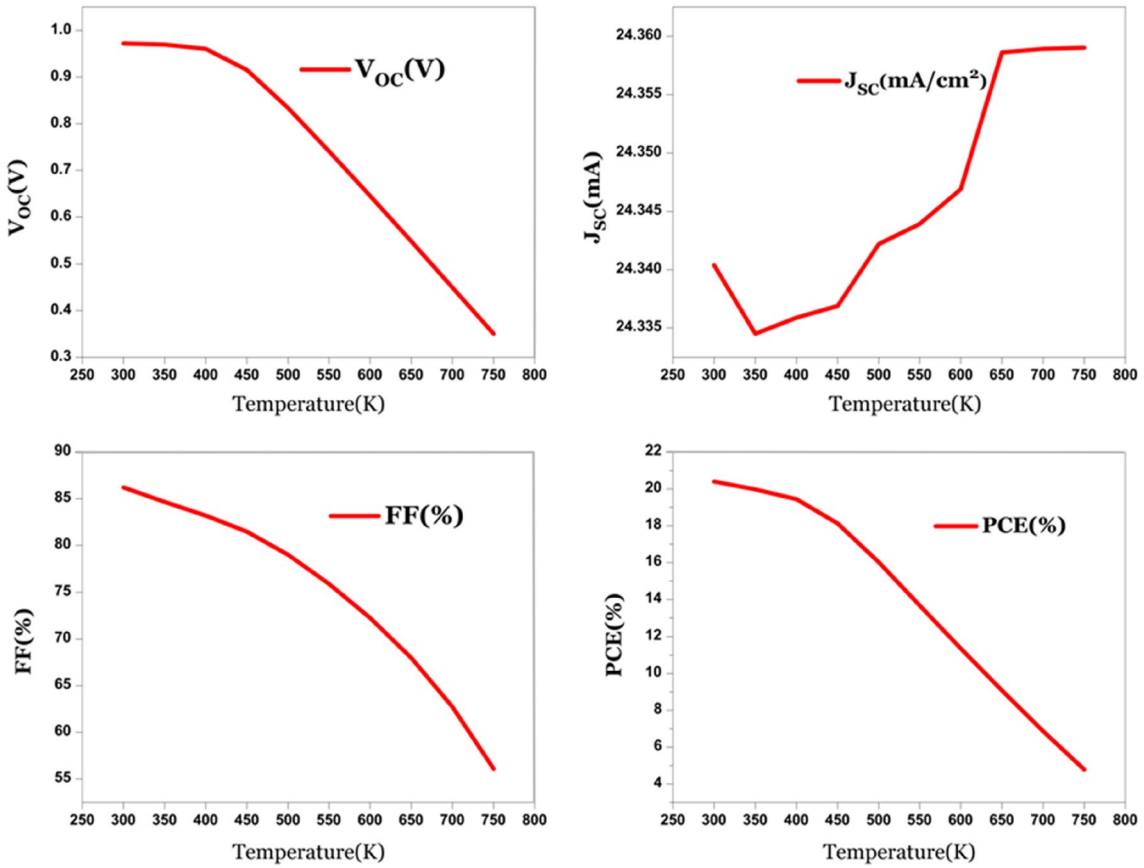

Fig. 10 Temperature effect on optimized device

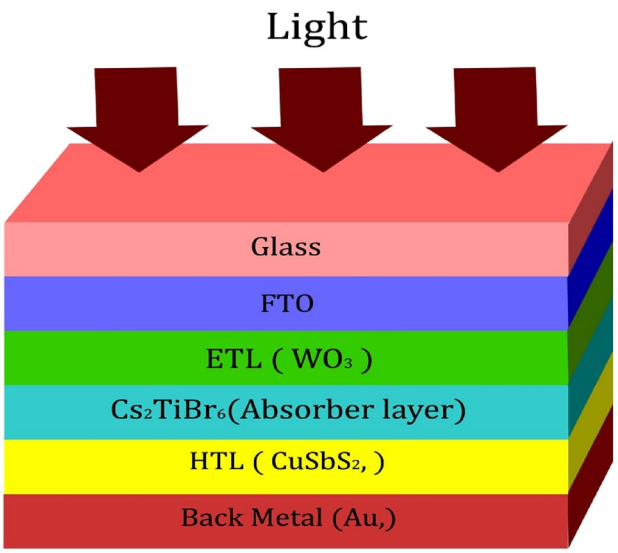

Fig. 11 Schematic diagram of novel design

solar cells is depicted in Fig. 10. From the plots, it is noticeable that the PCE, FF and Voc decrease with temperature. Hence, the PSC offers better performance at 300 k.

Optimized device

The novel optimized design is illustrated in Fig. 11. The quantum efficiency (Q.E) of a solar cell is a measure of the ratio of number of carriers it collects to the number of photons it receives. Sandwiched absorbing layers that can only absorb photons in the range of 790 nm can be more effective.

According to Fig. 12, more than 98% photons are alive having wavelength between 300 and 800 nm, and less than 2% has been recombined via other processes (Auger and SRH). Hence, the sandwiched layer at 300–800 nm absorbs virtually all incident photons to create electron–hole pairs and carriers with minimal recombination by the built-in field.

Figures 13 and 14 provide the details of the spectral response and J-V characteristic curves of the optimized device. Furthermore, the device also has an excellent spectral response, which is in the visible range, with the PCE of 20.40%, Jsc of 24.3404 mA/cm^2, Voc of 0.9717 V, and FF of 86.24%.

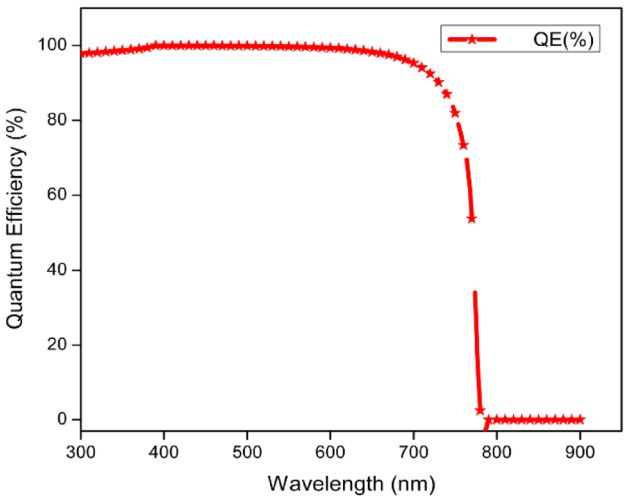

Fig. 12 Quantum efficiency of the Optimized PSC

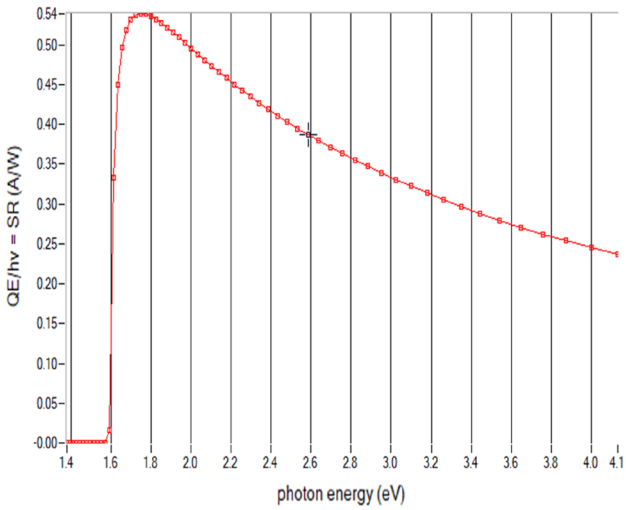

Fig. 13 Spectral response of optimized Device

Comparative analysis

Table 10 presents the comparison of existing Cs_2TiBr_6-based PSCs. This material is relatively new in the realm of PSCs, and it has received little research. From Table 10, we find that our optimized device performs better than existing works on Cs_2TiBr_6-based PSCs. This

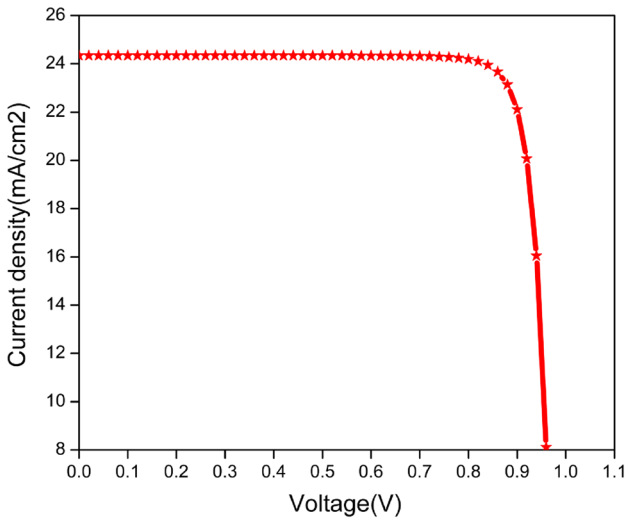

Fig. 14 J-V characteristics of optimized device

device appears to have comparatively favorable outcomes based on our test results, and it is ecologically friendly because it is a pure inorganic Ti-based perovskite, and it uses totally inorganic charge transport layers, the environment span end is projected to be extremely stable.

Conclusion

In this research, a lead-free, environmentally friendly, and stable Cs_2TiBr_6-based perovskite solar cell is presented, which integrates organic and inorganic charge transportation materials, in addition to different electron transport materials and metal contacts. By carefully selecting the HTL, ETL, back metal contacts, as well as the parameters of the absorb layer, which includes thickness and defect density, the device attains maximum performance and appears stable at 300 K. Despite using several back contact metals, the device has the maximum effectiveness with Au with a work function of 5.1 eV. Optimized solar cells retain their QE of 98% nearly at 800 nm wavelength. Analysis of the consequences of diverse HTL and ETL materials on invention enactment and optimization of layer thickness, back metal contacts and temperature caused in the evolution of an innovative high-performance combination of FTO/WO_3/Cs_2TiBr_6/Cu_2SbS_2/Au. This proposed system displays a peak PCE of 20.40%, a J_{SC} of 24.3042 mA/cm^2, V_{OC} of 0.9717 V, and a FF of 86.24%, also a QE of 98% at the visible spectrum. Designing lead-free, eco-friendly Ti-based PCS for future technologies may benefit from the proposed work.

Table 10 Performance comparison of existing Cs2TiBr6-based PSC

Structure	Jsc (mA/cm^2)	Voc (V)	FF (%)	PCE (%)	References
FTO/TiO_2/Cs_2TiBr_6/P_3HT/Au	3.87	0.89	59.5	2.25	Chen et al. (2018)
FTO/TiO_2/C_{60}/Cs_2TiBr_6/P_3HT/Au	5.75	0.99	54.9	3.12	Chen et al. (2018)
CuSCN/ Cs_2TiBr_6/CdS/Si	8.9			6.68	Chakraborty et al (2019)
FTO/TiO_2/Cs_2TiBr_6/NiO/Au	10.25	1.12	73.59	8.51	Samanta et al. (2020)
FTO/SnO_2/ Cs_2TiBr_6/MoO_3/Au	8.66	1.53	86.45	11.49	Zuo and Ding 2015)
ATO/TiO_2/Cs_2TiBr_6/NiO/Au	–	–	–	17.83	Moiz et al. (2021)
Proposed FTO/WO_3/Cs_2TiBr_6/Cu_2SbS_2/Au	24.3404	0.97	86.24	20.40	

Declarations

Conflict of interest No conflict of interest.

References

Ahmed S, Jannat F, Abdul Kaium Khan MD, Alim MA (2021) Numerical development of eco-friendly Cs_2TiBr_6 based perovskite solar cell with all-inorganic charge transport materials via SCAPS-1D. Int J Light Electron Optics 225:165765

Alam I, Mollick R, Ashraf MA (2021) Numerical simulation of $Cs_2AgBiBr_6$-based perovskite solar cell with ZnO nanorod and P3HT as the charge transport layers. Phys B Condens Matter 618:413187

Alam I, Ashraf MA (2020) Effect of different device parameters on tin-based perovskite solar cell coupled with In_2S_3 electron transport layer and CuSCN and Spiro-OMeTAD alternative hole transport layers for high-efficiency performance. Energy Sources Part A Recover Util Environ Effects

Ameri M, Mohajerani E, Ghafarkani M, Safari N, Alavi SA (2019) The investigation of the unseen interrelationship of grain size, ionic defects, device physics and performance of perovskite solar cells. J Phys D Appl Phys 52:125501

Atowar Rahman M (2022) Numerical modeling of ultra-thin CuSbS2 heterojunction solar cell with TiO2 electron transport and CuAlO2: Mg BSF layers. Opt Mater Express 12:2954

Babayigit A, Ethirajan A, Muller M, Conings B (2016) Toxicity of organometal halide perovskite solar cells. Nat Mater 15:247–251

Behrouznejad F, Shahbazi S, Taghavinia N, Wu H-P, Wei-Guang Diau E (2016) A study on utilizing different metals as the back contact of $CH_3NH_3PbI_3$ perovskite solar cells. J Mater Chem A 4:13488–13498

Burgelman M, Nollet P, Degrave S (2000) 'Modelling polycrystalline semiconductor solar cells.' Thin Solid Films 6:361–362

Chakraborty K, Choudhury MG, Paul S (2019) Numerical study of Cs_2TiX_6(X = Br−, I−, F− and Cl−) based perovskite solar cell using SCAPS-1D device simulation. Solar Energy 194:886–892

Chen K, Hu Q, Liu T, Zhao L, Luo D, Wu J, Zhang Y, Zhang W, Liu F, Russell TP, Zhu R, Gong Q (2016) 'Charge-carrier balance for highly efficient inverted planar heterojunction perovskite solar cells.' Adv Mater 28(48):10718–10724

Chen M, Ju M-G, Carl A, Zong Y, Grimm RL, Gu J, Zeng XC, Zhou Y, Padture NP (2018) Cesium Titanium (IV) bromide thin films based stable lead-free perovskite solar cells. Joule 2:558–570

Deepthi Jayan K, Sebastian V (2021) Comprehensive device modelling and performance analysis of MASnI3 based perovskite solar cells with diverse ETM, HTM and back metal contacts. Sol Energy 217:40–48

DivyaSharma RajeshMehra (2022) BalwinderRaj, Optimization of tin based perovskite solar cell employing CuSbS2 as HTL: A numerical simulation approach. Opt Mater 134:113060

Du HJ, Wei-Chao W, Jian-Zhuo Z (2016) Device simulation of lead-free $CH_3NH_3SnI_3$ perovskite solar cells with high efficiency. Chin Phys B 25(10):108802

Giordano F, Abate A, Baena JPC, Saliba M, Matsui T, Im SH, Zakeeruddin SM, Nazeeruddin MK, Hagfeldt A, Graetzel M (2016) Enhanced electronic properties in mesoporous TiO_2 via lithium doping for high-efficiency perovskite solar cells. Nat Commun 7:10379

Giustino F, Snaith HJ (2016) Toward, lead-free perovskite solar cells. ACS Energy Lett 1(6):1233–1240

Grandhi G, Matuhina A, Liu M, Annurakshita S, Ali-Löytty H, Bautista G, Vivo P (2021) Lead-free cesium titanium bromide double perovskite nanocrystals. Nanomaterials 11:1458

Green MA (2009) The path to 25% silicon solar cell efficiency: History of silicon cell evolution. Prog Photovolt Res Appl 17:183–189

Gu PY, Wang N, Wu A, Wang Z, Tian M, Fu Z, Sun XW, Zhang Q (2016) An azaacene derivative as promising electron-transport layer for inverted perovskite solar cells. Chem Asian J 11:2135–2138

Huan L, Sun X, Li C, Xu R, Xu J, Du Y, Wu Y, Ni J, Cai H, Li J (2016) Electron transport layer-free planar perovskite solar cells: further performance enhancement perspective from device simulation. Sol Energy Mater Sol Cells 157:1038–1047

Ju M-G, Chen M, Zhou Y, Garces HF, Dai J, Ma L, Padture NP, Zeng XC (2018) Earth-abundant nontoxic titanium(IV)-based vacancy-ordered double perovskite halides with tunable 1.0 to 1.8 eV bandgaps for photovoltaic applications. ACS Energy Lett 3:297–304

Kabir E, Kumar P, Kumar S, Adelodun AA, Kim K-H (2018) 'Solar energy: Potential and future prospects.' Renew Sustain Energy Rev 82:894–900

Kim GH, Kim DS (2021) Development of perovskite solar cells with >25% conversion efficiency. Joule 5(5):1033–1035

Lakhdar N (2020) Hima, Abdelkader, electron transport material effect on performance of perovskite solar cells based on $CH_3NH_3GeI_3$. Opt Mater 99:109517

Mehrabian M, Afsha EN, Yousefzadeh SA (2021) Simulating the thickness effect of the graphene oxide layer in CsPbBr 3- based solar cells Masood. Mater Res Express 8:035509

Moiz SA, Alahmadi ANM, Aliohani AJ (2021) Design of a novel lead-free perovskite solar cell for 17.83% efficiency. IEEE Access 9:54254–54263

Mottakin M et al (2021) Design and modelling of eco-friendly $CH_3NH_3SnI_3$-based perovskite solar cells with suitable transport layers. Energies 14:7200

Najafi M, Di Giacomo F, Zhang D, Shanmugam S, Senes A, Verhees W, Hadipour A, Galagan Y, Aernouts T, Veenstra S (2018) Highly efficient and stable flexible perovskite solar cells with metal oxides nanoparticle charge extraction layers. Nano. Micro Small 14:1702775

Otoufi MK, Ranjbar M, Kermanpur A, Taghavinia N (2020) Enhanced performance of planar perovskite solar cells using TiO_2/SnO_2 and TiO_2/WO_3 bilayer structures: Roles of the interfacial layers. Sol Energy 208:697–707

Ouslimane T, Et-taya L (2021) Lahoucine Elmaimouni, Abdellah Benami, Impact of absorber layer thickness, defect density, and operating temperature on the performance of MAPbI3 solar cells based on ZnO electron transporting material. Heliyon 7:e06379

Pecunia V, Occhipinti LG, Chakraborty A, Pan Y, Peng Y (2020) Lead-free halide perovskite photovoltaics: Challenges, open questions, and opportunities. APL Mater 8:100901

Pitchaiya S, Natarajan M, Santhanam A, Asokan V, Yuvapragasam A, Ramakrishnan VM, Palanisamy SE, Sundaram S, Velauthapillai D (2020) 'A review on the classification of organic/inorganic/carbonaceous hole transporting materials for perovskite solar cell application.' Arabian J Chem 13(1):2526–2557

Pizzini S (2010) Towards solar grade silicon: Challenges and benefits for low cost photovoltaics. Sol Energy Mater Sol Cells 94:1528–1533

Rafsun Jani MD et al (2020) Exploring Solar Cell Performance of Inorganic Cs2TiBr 6 Halide Double Perovskite: A Numerical Study. Superlattices Microstruct 146:106652

Rai N, Rai S, Singh PK, Pooja Lohia DK, Dwivedi, (2020) Analysis of various ETL materials for an efficient perovskite solar cell by numerical simulation. J Mater Sci Mater Electron 31:16269–16280

Said AA, Xie J, Zhang Q (2019) Recent progress in organic electron transport materials in inverted perovskite solar cells. Small 15:1900854

Samanta M, Ahmed SI, Chattopadhyay KK, Bose C (2020) Role of various transport layer and electrode materials in enhancing performance of stable environment-friendly Cs_2TiBr_6 solar cell. Optik Int J Light Electron Optics 217:164805

Shivesh K, Alam I, Kushwaha AK, Kumar M, Singh SV (2021) Investigating the theoretical performance of Cs_2TiBr_6-based perovskite solar cell with La-doped $BaSnO_3$ and $CuSbS_2$ as the charge transport layers. Int J Energy Res 46:6045–6064

Slami A, Bouchaour M, Merad L (2019) Numerical Study of Based Perovskite Solar Cells by SCAPS-1D. Int J Energy Environ 13:17–21

Tohidul Islam Md, Rafsun Jani Md, Shorowordi K, Hoque Z, Gokcek AM, Vattipally V, Nishat SS, Ahmed S (2021) Numerical simulation studies of $Cs_3Bi_2I_9$ perovskite solar device with optimal selection of electron and hole transport layers. Optik 231:166417

Verschraegen J, Burgelman M (2007) 'Numerical modeling of intraband tunneling for heterojunction solar cells in SCAPS.' Thin Solid Films 515(15):6276–6279

Wang J, Zhenming X (2017) Environmental friendly technology for aluminum electrolytic capacitors recycling from waste printed circuit boards. J Hazard Mater 326:1–9

Wang T, Li YY, Mitzi DB (2020) Is Cs_2TiBr_6 a promising Pb-free perovskite for solar energy applications? J Mater Chem A 8:2–7

Wang K, Olthof S, Subhani WS, Jiang X, Cao Y, Duan L, Wang H, Du M, Liu SF (2020) Novel inorganic electron transport layers for planar perovskite solar cells: Progress and prospective. Nano Energy 68:104289

Yang Bo, Wang L, Han J, Zhou Y, Song H, Chen S, Jie Zhong Lu, Lv DN, Tang J (2014) $CuSbS_2$ as a promising earth-abundant photovoltaic absorber material: a combined theoretical and experimental study. Chem Mater 26:3135–3143

Zuo C, Ding L (2015) Solution-processed Cu_2O and CuO as whole transport materials for efficient perovskite solar cells. Epub 11(41):5528–5532